

Deep-Imaging Observations of a Candidate of an Absorbed QSO at $z = 0.653$, AX J131831+3341

Masayuki AKIYAMA,¹ Kouji OHTA,²*Naoyuki TAMURA,²*Mamoru DOI,^{3,4}

Masahiko KIMURA,⁵ Yutaka KOMIYAMA,¹ Satoshi MIYAZAKI,⁶ Fumiaki NAKATA,³

Sadanori OKAMURA,^{3,4} Maki SEKIGUCHI,⁷ Kazuhiro SHIMASAKU,^{3,4} Masafumi YAGI,⁸

Masaru HAMABE,⁹ Michitoshi YOSHIDA,¹⁰ and Tadahumi TAKATA,¹

¹ *Subaru Telescope, National Astronomical Observatory of Japan,
650 North A'ohoku Place, Hilo, HI 96720, U.S.A*

E-mail(MA): akiyama@naoj.org

² *Department of Astronomy, Faculty of Science, Kyoto University, Kyoto 606-8502*

³ *Department of Astronomy, School of Science, The University of Tokyo, Bunkyo-ku, Tokyo 113-0033*

⁴ *Research Center for the Early Universe, School of Science,
The University of Tokyo, Bunkyo-ku, Tokyo 113-0033*

⁵ *Department of Physics, School of Science, The University of Tokyo, Bunkyo-ku, Tokyo 113-0033*

⁶ *Advanced Technology Center, National Astronomical Observatory, Mitaka, Tokyo 181-8588*

⁷ *Institute for Cosmic Ray Research, The University of Tokyo, Tanashi, Tokyo 188-8502*

⁸ *Optical and Infrared Astronomy Division, National Astronomical Observatory,
Mitaka, Tokyo 181-8588*

⁹ *Institute of Astronomy, School of Science, The University of Tokyo, Mitaka, Tokyo 181-0015*

¹⁰ *Okayama Astrophysical Observatory, National Astronomical Observatory,
Kamogata-cho, Okayama 719-0232*

(Received 2000 January 11; accepted 2000 June 6)

Abstract

The results of deep-imaging observations of a candidate of an absorbed QSO at $z = 0.653$,

AX J131831+3341, are presented. AX J131831+3341 was found during the course of optical follow-up observations of the ASCA Large Sky Survey, and has an X-ray luminosity of 10^{45} erg s $^{-1}$ (2–10 keV), which corresponds to those of QSOs. Its optical spectrum shows no significant broad H β emission line, suggesting that the object is an absorbed QSO. Deep R and V band images reveal the presence of a point-like nucleus and an asymmetric extended component. The nuclear component has a blue color, and the optical magnitude is much fainter than that expected from the observed X-ray flux for typical type-1 AGNs. These photometric properties and the presence of broad Mg II 2800 Å emission can be explained simultaneously if the observed nuclear light is dominated by scattered nuclear light, though there is a possibility that the nuclear component is a slightly absorbed nucleus if its intrinsic X-ray to optical flux ratio is the largest among X-ray selected AGNs. The size of the extended component, which is thought to be the host galaxy of the QSO, is larger than those of normal disk galaxies at $z = 0 - 0.75$, and the absolute magnitude is similar to those of the brightest host galaxies of QSOs at redshifts smaller than 0.5. The $V - R$ and $R - I$ colors of the component are consistent with a 1 Gyr-old stellar population model without absorption.

Key words: galaxies: active — galaxies: individual (AX J131831+3341) — galaxies: photometry — quasars

1. Introduction

AX J131831+3341 is an AGN at a redshift of 0.653, discovered during the optical identification of hard X-ray sources in the ASCA Large Sky Survey (LSS; Akiyama et al. 2000, hereafter Paper I). The optical spectrum of the object shows strong emission lines, such as broad Mg II 2800 Å, narrow [O II] 3727 Å, and narrow [O III] 5007 Å, but no broad H β emission line. Its small H β -to-[O III] 5007 Å equivalent width ratio [$\log(H\beta/[O\ III]) = -0.54$] is comparable to those of Seyfert 1.8–2 galaxies (Winkler 1992).

The X-ray flux of the object is 5.8×10^{-13} erg cm $^{-2}$ s $^{-1}$ in a 2–10 keV band and the luminosity is estimated to be 10^{45} erg s $^{-1}$, which is as large as the luminosity of the knee of the AGN luminosity function in the 2–10 keV band at $z \sim 0.6$ (e.g., Boyle et al. 1998), and corresponds to the luminosities of QSOs. The observed X-ray spectrum of the object in a 0.7–10 keV band is described by intrinsic absorption with a hydrogen column density of

* Visiting astronomer of the University of Hawaii 88" telescope.

$N_{\text{H}} = 6.0_{-4.2}^{+4.4} \times 10^{21} \text{ cm}^{-2}$ and an intrinsic photon index of 1.7, which is typical for broad-line AGNs. The hydrogen column density corresponds to the lower edge of the column density distribution of Seyfert 1.8–1.9 galaxies (Risaliti et al. 1999).

AX J131831+3341 is detected as a point source in the FIRST radio source survey (Becker et al. 1995) in the 1.4 GHz band with a flux density of 2.0 mJy; the calculated radio power of the object, $L_{1.4\text{GHz}}$, is $4 \times 10^{24} \text{ W Hz}^{-1}$. The X-ray to radio-flux ratio of the object is 100-times larger than those of radio-loud AGNs, and similar to the upper envelope of radio-quiet AGNs in the ASCA LSS sample (Paper I). Therefore, AX J131831+3341 is a good candidate of a radio-quiet absorbed luminous AGN (absorbed QSO) at an intermediate redshift.

Absorbed QSOs whose luminous nuclear optical emissions are obscured make it possible to detect faint and small nebulosities around QSOs and provide a unique opportunity to examine the nature of host galaxies of a radio-quiet QSO population. In fact, an optical image of the object taken without a filter for object acquisition during a spectroscopic observation shows a faint nebulosity around a point-like component. The faint nebulosity extends $\sim 7''$ from the nucleus (Paper I). Since most of host galaxy imagings of radio-quiet QSOs by Hubble Space Telescope are limited below a redshift of ~ 0.5 (e.g., Bahcall et al. 1997; Boyce et al. 1998; Hooper et al. 1997; McLure et al. 1999), the X-ray selected absorbed QSO is a precious site for studying host galaxies of radio-quiet QSOs, especially in the intermediate-to-high redshift universe. In this paper, we present results of optical photometric and deep imaging observations of AX J131831+3341, and discuss the possibility that the object is an absorbed QSO as well as the properties of its host galaxy. Throughout this paper, we use $q_0 = 0.5$ and $H_0 = 50 \text{ km s}^{-1} \text{ Mpc}^{-1}$.

2. Observations

Deep optical imaging observations were made with the Suprime-Cam attached to the Cassegrain focus of the 8.2 m Subaru telescope on 1999 May 13, June 11, and June 12 during the first-light phase of the telescope. The camera consisted of 6 4096×2048 CCD chips. For the observation, a SITe 4096×2048 chip was used. The pixel scale of the camera was $0.''03 \text{ pixel}^{-1}$. The seeing condition during the observation was not very good (FWHM is $\sim 0.''7$). Three 600 s exposures in the R band and two 900 s exposures in the V band were obtained. Unfortunately, because the object fell at an edge of the CCD in one frame in each band, the northern part of the image in the R band and the southern part of the image in the V band were observed with shorter effective exposure times than the other region.

Photometric calibrations of the V and R band images were performed based on optical photometric observations made with the Tektronix 2048×2048 CCD at the University of Hawaii (UH) $88''$ telescope on 1999 March 6. We obtained Mould V and R band images with exposure times of 450 s and 1500 s, respectively. During the observing run, 50 Landolt's standard stars (Landolt 1992) were observed. The seeing size was $\sim 0.''8$ and the pixel scale was $0.''22$ pixel $^{-1}$. In the observation, we also obtained Mould B and I band images with 600 s and 300 s exposures, respectively.

All of the deep imaging and photometric data were analyzed using IRAF. Bias subtraction and flat-fielding with dome flats were performed. Based on the scatters of the countrate-to-magnitude conversion factors of the observed Landolt's standard stars, the uncertainties in the photometric calibrations were estimated to be 0.03, 0.06, 0.03, and 0.06 mag in the B , V , R , and I bands, respectively. The photometric calibrations of the deep Subaru images were made with bright stars whose magnitudes were measured in the UH $88''$ images.

3. Results

3.1. Morphology

The deep R band image of AX J131831+3341 is shown in figure 1. We binned the original image in 4×4 pixels. The standard deviation in the sky region of the V and R band deep images are 0.03 and 0.04 counts s $^{-1}$ per 4×4 binned pixels, which correspond to 26.47 and 26.07 mag arcsec $^{-2}$, respectively. In figure 1, we show a sky-subtracted image of the object with the surface brightness ranging from -3 times the standard deviation to $+9$ times the standard deviation as a gray scale with a linear scale.

The galaxy has a point-like nucleus and a peculiar extended component. The profile of the nucleus is well represented by the point spread function (PSF) in the image. The peculiar structure extends $\sim 8''$ away from the nuclear component. The structure has an asymmetric feature: it extends more in the southeastern direction than in the northwestern direction. In the southeastern region, there is a gap running from the center to the edge of the component. An extended structure is also detected in the V and I band images.

3.2. Total Magnitudes

Based on the images taken with the UH $88''$ telescope, the magnitudes of AX J131831+3341 are measured in a $26.''4$ aperture centered on the nucleus excluding objects around AX J131831+3341 and a knot located at $\sim 10''$

northwest from the nucleus. The resulting magnitudes are 21.23 ± 0.10 , 21.08 ± 0.13 , 20.00 ± 0.10 , and 18.96 ± 0.13 mag in the B , V , R , and I bands, respectively. The photometric uncertainties include not only the uncertainties of the flux calibrations (see subsection 2.1), but also errors of flat-fielding and uncertainties of sky subtractions (0.1 mag in the all bands). In the deep V and R -band images obtained with Subaru, the total magnitudes of AX J131831+3341 were measured to be 21.06 ± 0.1 and 20.04 ± 0.1 mag in the V and R bands with the same aperture, respectively. These magnitudes agree with those derived from UH photometric observations. The results are summarized in table 1. Hereafter, we use the V and R -band magnitudes from Subaru observations and the B and I -band magnitudes from UH 88" observations.

3.3. Colors and Magnitudes of the Extended and the Nuclear Component

To evaluate the magnitudes and colors of the extended component, we measured them within regions A and B shown in figure 1 using the deep Subaru V and R -band images and the UH 88" I -band image. The magnitudes in region A (B) are 22.91 (23.24) mag in the V band, 21.90 (22.14) mag in the R band, and 21.10 (20.92) mag in the I band. The uncertainty of the photometry is 0.1 mag in the V and R bands and 0.15 mag in the I band. Thus, the colors in region A (B) are estimated to be $V - R$ of 1.01 (1.10) ± 0.14 mag and $R - I$ color of 0.80 (1.22) ± 0.18 mag.

To derive the photometric parameters of the nuclear and extended components separately, we deconvolved the two components using the surface-brightness profile of the object. Since the object has asymmetric and complex features, we decided to model the surface-brightness distribution of the galaxy to obtain a rather symmetric and smooth brightness distribution as follows. We first fitted ellipses, of which the centers, position angles, ellipticities, and surface brightnesses were free parameters, to the isophotes of the object, using the **ellipse** command of the **isophot** package in the IRAF. The sampling step of the ellipses changes with the semi-major axis length; the step size is taken to be one twelfth of the semi-major length of each ellipse. Next, based on the fitted parameters, we constructed a model image of the galaxy with **bmodel** command of the above package. The R -band image of the constructed model and the residual image after subtracting the model from the original image are shown in figure 2. (Figure 2 is shown in the same count rate range as that used in figure 1.) As can be seen in figure 2, the constructed model well describes the overall shape of the original image. The total magnitude of the residual image is 22.0 mag, which corresponds to 16% of the total magnitudes. The method was applied not only to the deep V and R images,

but also to the *I*-band image in which the extended component is also detected.

The surface brightness profiles are derived as sections of the model image along the major-axis (position angle of 114°), and are shown in figure 3. The derived profiles are consistent with the cross sections along the major axis of the object, though they are not as smooth as expected from the image. Figure 3 shows that the extended component follows the exponential profile, which is typical for galactic disks. In both the *V* and *R*-band profiles, in the inner region ($r \leq 4''$), the profiles in the southeastern and northwestern directions agree with each other within the uncertainties of the model fittings, while in the outer region ($r \geq 4''$) the southeastern component is brighter than the northwestern component. The exponential law is fitted to the profiles in the regions from $1.''5$ to $4''$ in both the *V* and *R*-bands. The best-fit profiles are $\mu_V = 24.73 + 0.24 r('')$ and $\mu_R = 23.41 + 0.36 r('')$ (mag arcsec $^{-2}$) for the southeastern direction and $\mu_V = 24.52 + 0.34 r('')$ and $\mu_R = 23.61 + 0.24 r('')$ (mag arcsec $^{-2}$) for the northwestern direction. The fitting uncertainties of the central surface brightness and the disk scale lengths are ~ 0.2 mag arcsec $^{-2}$ and $0.''5 - 1''$, respectively. By subtracting the fitted exponential profiles in the southeastern (northwestern) direction from the original profile, the profiles of the nuclear component are obtained in each direction. Since the obtained profiles agree well with the PSF in each band, which is derived by averaging the profiles of stellar objects, we fitted the PSF to the residual profiles. The dashed lines in figure 3 represent the summed profiles of the best-fit PSFs and the best-fit exponential laws in the *V* and *R*-bands. Since these deconvolutions reproduce the observed profiles satisfactorily in each band, we did not undertake an iteration of the profile-fitting process, and adopted these fitting results as the final ones. We applied the same deconvolution method to the *I*-band image, assuming that its scale length to be the same as that in the *R*-band image, and that the extended component dominates the surface brightness in the range between $1.''5$ and $2''$.

The magnitudes of the resulting nuclear components were calculated to be 22.61 (22.64), 22.26 (22.22), and 21.77 (21.66) mag in the *V*, *R*, and *I* bands, respectively. (The values in parentheses denote those determined from the northwestern profile.) Because the central surface brightnesses are dominated by the nuclear component, the magnitudes derived from the southeastern and northwestern profiles agree well. The uncertainty of the magnitude of the nuclear component is dominated by that of the photometric calibration and sky subtraction (0.1 mag in the *V* and *R* band and 0.13 mag in the *I* band). We list the derived values in the southeastern region in table 1. Hereafter, we refer to these magnitudes as those of the nuclear component. Subtraction of the magnitudes of the nuclear component from the total magnitudes of AX J131831+3341 gives the magnitudes of the extended components:

21.36, 20.19, and 19.04 mag in the V , R , and I bands, respectively. The nuclear component contributes 24% in the V band, 13% in the R band, and 8% in the I band of the total flux; thus, the contribution from the extended component dominates the total magnitudes of AX J131831+3341 in these bands. From these magnitudes, the colors of the extended component are estimated to be $V - R = 1.17 \pm 0.14$ mag and $R - I = 1.15 \pm 0.16$ mag.

4. Discussions

4.1. Nature of the Nuclear Component

The nuclear component should be related to the AGN; strong broad Mg II 2800 Å emission line is detected and the rest-frame equivalent width of the broad line (99 ± 25 Å) is larger than those of normal QSOs (50 ± 29 Å ; Francis et al. 1991), implying that the nuclear component is dominated by AGN light, at least in the B band. Possible explanations for the origin of nuclear light are that we see either an absorbed AGN directly or scattered AGN light.

Regarding the first case, if we assume that the nucleus has the same intrinsic X-ray to optical flux ratio of soft X-ray selected AGNs/QSOs [$\log(f_{X_{0.3-3.5\text{keV}}}/f_V)$ values of Einstein Medium Sensitivity Survey (hereafter EMSS) AGNs range from -1.0 to $+1.4$ and peak at $+0.2$; Stocke et al. 1991] and a typical photon index of type 1 AGNs (1.7), it should appear with a magnitude of $14.5 - 20.5$ mag in the R band. If the object has a typical X-ray to optical flux ratio [$\log(f_{X_{0.3-3.5\text{keV}}}/f_V) = +0.2$], it should have a magnitude of 17.5 mag in the R band. The observed R -band magnitude of the nuclear component is much fainter than the magnitude range. It should be noted that BL Lac objects have a larger $\log(f_{X_{0.3-3.5\text{keV}}}/f_V)$ value ($+0.3$ to $+1.7$; Stocke et al. 1991) than normal AGNs/QSOs; but, AX J131831+3341 is not such an object, because it is not a radio-loud AGN. If the absorption causes the faintness of the nuclear component, an optical extinction larger than 1.76 mag at 4000 Å to the nucleus is required. The optical extinction corresponds to A_V of larger than 1.2 mag, based on the extinction curve of the Galaxy (e.g., Scheffler, Elsässer 1988). If the object intrinsically has the typical X-ray to optical flux ratio, the optical extinction to the nucleus is estimated to be $A_V = 3.3$ mag. The derived range of the optical extinction is consistent with that derived from X-ray spectral fitting ($A_V = 3.4^{+2.5}_{-2.3}$ mag, if we assume the correlation of X-ray absorption and optical absorption in the galactic interstellar gas (e.g., Predehl, Schmitt 1995)). The expected range of colors of the average QSO SED absorbed with A_V between 1.1 mag and 5.9 mag is indicated by the dashed line in figure 4. The $V - R$ and $R - I$ colors of the nuclear component are marginally consistent with those of an averaged QSO SED (Francis et

al. 1991) if A_V is about 1.0 mag, but much bluer than the QSO SED with $A_V = 3.3$ mag. Thus, only if the intrinsic X-ray to optical flux ratio of the object is the largest among the X-ray selected AGNs (and thus in the minimum extinction case), the large X-ray to optical flux ratio and blue colors of the nuclear component can be explained simultaneously.

In narrow-line AGNs, some fraction of the nuclear light is scattered into our line of sight by dust particles or electrons. In narrow-line radio galaxies, the fraction is estimated to be a few percent based on spectropolarimetric observations (Alighieri et al. 1994). Such scattered light from an obscured AGN can dominate the optical light of an object, especially in the wavelength range below the rest-frame 4000 Å, if the obscured AGN is intrinsically as luminous as the QSOs and the host has a red color, like that of an elliptical galaxy. For AX J131831+3341, assuming that the nucleus has the same intrinsic optical to X-ray flux ratio of AGNs in the EMSS sample and that 2 % of the nuclear light is scattered isotropically, the scattered component should appear with 18.7 – 24.7 mag in the R band. The observed R -band magnitude of the nuclear component falls in the magnitude range. The $V - R$, and $R - I$ colors are consistent with $f_\nu \sim \nu^{-1.0}$ and the $f_\nu \sim \text{constant}$ model with an A_V smaller than 1 mag. Such colors are similar to those of the scattered-light component in 3C radio galaxies (Alighieri et al. 1994). Therefore, the scattered AGN light can be the origin of the nuclear component.

The X-ray to Mg II 2800 Å flux ratio of AX J131831+3341 does not conflict with both models; the equivalent width of the broad line is similar to that of normal QSOs and the X-ray to optical flux ratio is explained by the two models. A broad Mg II 2800 Å emission line found in narrow-line radio galaxies (Alighieri et al. 1994; Barcons et al. 1998) and narrow-line ultra-luminous infrared galaxies (Hines, Wills 1993; Hines et al. 1995) is thought to originate from scattered nuclear light. Non-detection of a broad H β line can be explained by dilution of the nuclear emission by the host-galaxy component in a red wavelength range (see e.g., figure 5 in Alighieri et al. 1994, figure 3 in Willott et al. 2000) in the case of the scattered-light origin.

4.2. Nature of the Extended Component

The extended component is considered to be the host galaxy of the QSO. The asymmetric and extended structure of the component suggests a galaxy interaction or merging in the host galaxy. The gap, which runs from the center to the edge in the eastern extension, could be a dust lane in the component, or the component could consist of two tidal tails. The morphology of the component is similar to that of an interacting galaxy, NGC 2992, though the

extension of AX J131831+3341 ($\sim 8''$ corresponds to 62 kpc at $z = 0.653$) is much larger than that of NGC 2992 (20 kpc away from the nucleus; Ward et al. 1980). Similar extended tails can be seen in some Ultra Luminous Infrared Galaxies (ULIGs, Sanders et al. 1988). It is also possible that we see an edge-on disk galaxy with an asymmetric dust lane.

We compared the colors of the extended component (region A, region B, and total–nucleus) with spectral evolution models of the galaxies in figure 4. We used two models (Kodama, Arimoto 1997): 1) Elliptical model (plotted with a solid line) in which star formation occurs during the first 0.353 Gyr with an initial mass function with a slope of 1.20; after that the galaxy evolves passively. The model parameters well reproduce the reddest and brightest ($M_V = -23$) class elliptical galaxy in the Coma cluster (Kodama et al. 1998). 2) Disk model (plotted with a dotted line) is used in which star formation occurs constantly with the same initial-mass function as that in the elliptical model. The colors of these models at ages from 0.01 Gyr to 12 Gyr at a redshift of 0.653 are shown as tracks. We mark the positions of models with 6 Gyr age with tick marks on the tracks of both models. The age corresponds to that of the universe at a redshift of 0.653 under the adopted cosmological parameters of $q_0 = 0.5$ and $H_0 = 50$ km s $^{-1}$ Mpc $^{-1}$. The colors of the extended component fall on the track of an elliptical model with an age of 0.5 – 1 Gyr, and the host galaxy is significantly bluer than the old 6 Gyr elliptical galaxy model in the $R - I$ color. Because the 0.5 – 1 Gyr elliptical model spectrum resembles that of a post-starburst galaxy, AX J131831+3341 may have a post-starburst galaxy as the host like “post-starburst quasar”, UN J1025–0040 (Brotherton et al. 1999), which is found at a redshift of 0.6344. If we introduce optical extinction in the host galaxy, the colors are also explained by a disk model or an elliptical or disk model at ages of less than 0.1 Gyr with an absorption of $A_V = 1 - 3$ mag.

From the R -band magnitude, which nearly corresponds to the B band in the object rest frame, the absolute magnitude of the extended component is estimated to be $M_B = -22.8$ mag, $M_V = -24.1$ mag, and $M_R = -23.7$ mag with a K -correction of 0.127 mag in the R band, $B - R$ color of 0.88 mag, and $V - R$ color of 0.41 mag in the object rest frame, based on the 1 Gyr elliptical model. It should be noted that since the B , V , R , and I bands in the observer’s frame cover the B and V bands in the object frame, the rest frame $V - R$ color is an extrapolation of the best-fit model in the observed range. The absolute magnitudes are ~ 2 mag brighter than that of the knee of the galaxy luminosity function at the object’s redshift ($M_B^* \sim -21$ mag; Lilly et al. 1995), and correspond to the brightest host galaxies of QSOs at a redshift less than 0.5 observed with the Hubble Space Telescope ($M_R = -22.5 - -24.5$ mag, McLure et al. 1999; $M_R = -22.24 - -23.97$ mag, Hooper et al. 1997;

$M_V = -20.5 - -23.5$ mag, Bahcall et al. 1997). The absolute magnitude also matches the brightest ULIG in the intermediate redshift ($z \sim 0.2$) universe ($M_R = -21.9 - -23.7$, Zheng et al. 1999, assuming $R - I$ color of an elliptical galaxy as 0.7). The post-starburst nature could make the host galaxy brighter than the absolute magnitude of the knee of the galaxy luminosity function at the object redshift; the total magnitude in the observer's frame R band of the 1 Gyr elliptical galaxy model is 2.7 mag brighter than that of the 6 Gyr elliptical galaxy model having the same mass.

We compare the scale length and the central surface brightness of the host galaxy with those of normal galaxies, though the extended component may not be a normal disk of a galaxy. The disk scale lengths derived from the fitting made in section 3.3 are 4."1 and 3."0 in V band and 2."8 and 4."2 in R band for the southeastern and the northwestern directions, respectively. These values in the R band correspond to the scale lengths of 22 ± 8 kpc and 33 ± 8 kpc at the object redshift in the southeastern and northwestern direction, respectively. The lengths are larger than the largest disk scale length of nearby galaxies (~ 20 kpc; Kent 1985). The large extended feature resembles that of early-type galaxies (NGC 3872, NGC 5533) and interacting galaxies (NGC 2770, NGC 5905) in the sample by Kent (1985). Based on the observed central surface brightness of the extended component in the R band, that in the rest-frame B band is estimated to be 21.44 mag arcsec^{-2} by correcting for the $(1+z)^{-4}$ surface brightness dimming (2.18 mag arcsec^{-2}), K -corrections (0.67 mag) and the $B - R$ colors (0.88 mag) of the 1 Gyr elliptical model. The brightness corresponds to a typical value of the normal disk galaxies ($\mu_B = 20 - 23$ mag arcsec^{-2} ; Freeman 1970; Kent 1985) but brightest end of disks with a scale length of ~ 20 kpc. The obtained scale lengths are almost the largest among those of normal disk galaxies at $z = 0.5 - 0.75$; also, the central surface brightnesses are as bright as, or slightly fainter than, those of normal disk galaxies at $z = 0.5 - 0.75$ (Lilly et al. 1998).

In figure 5, we compared the surface brightness profile of AX J 131831+3341 with the best-fit profiles of the QSO host galaxies at $z \sim 0.2$ detected in observations with Hubble Space Telescope (McLure et al. 1999). In contrast to the exponential profile of AX J131831+3341, most of the observed profiles are well described by the de Vaucouleurs $r^{1/4}$ law, which is a typical profile of an elliptical galaxy and a bulge of a spiral galaxy. The best-fit profiles were converted from those at a redshift of ~ 0.2 to that at a redshift of 0.653 with surface-brightness dimming of $(1+z)^{-4}$ and a band-shift effect by using SED of an elliptical galaxy at $z = 0$ (~ 1 mag in R band), which represents their $R - K$ colors (McLure et al. 1999). We convolved these profiles with the PSF in our data. The extended component of AX J131831+3341 has a brighter surface brightness and a larger scale length than that of the QSO host galaxies.

Many absorbed radio-quiet QSOs, like AX J131831+3341, are expected to be found in optical follow-ups of hard X-ray surveys with new-generation X-ray satellites, Chandra and XMM-Newton observatories. Information on the morphological, photometric, and spectroscopic characteristics of the host galaxies of absorbed radio-quiet QSOs, especially at an intermediate-to-high redshift universe, will be an important key to understand the QSO populations, host galaxies of QSOs and connection between galaxy evolution and AGN evolution (e.g., Boyle, Terlevich 1998).

KO and NT appreciate the support from members of the UH observatory during the imaging observations. MA acknowledges support from Research Fellowships of the Japan Society for the Promotion of Science for Young Scientists. The optical follow-up program is supported by grants-in-aid from the Ministry of Education, Science, Sports and Culture (06640351, 08740171, 09740173) and from the Sumitomo Foundation.

References

- Akiyama M., Ohta K., Yamada T., Kashikawa N., Yagi M., Kawasaki W., Sakano M., Tsuru T. et al. 2000, ApJ 532, 700 (Paper I)
- Alighieri S.S., Cimatti A., Fosbury R.A.E. 1994, ApJ 431, 123
- Bahcall J.N., Kirhakos S., Saxe D.H., Schneider D.P. 1997, ApJ 479, 642
- Barcons X., Carballo R., Ceballos M.T., Warwick R.S., Gonzalez-Serrano J.I. 1998, MNRAS 301, L25
- Becker R.H., White R.L., Helfand D.J. 1995, ApJ 450, 559
- Boyce P.J., Disney M.J., Blades J.C., Boksenberg A., Crane P., Deharveng J.M., Macchetto F.D., Mackay C.D., Sparks W.B. 1998, MNRAS 298, 121
- Boyle B.J., Georgantopoulos I., Blair A.J., Stewart G.C., Griffiths R.E., Shanks T., Gunn K.F., Almaini O. 1998, MNRAS 296, 1
- Boyle B.J., Terlevich R.J. 1998, MNRAS 293, L49
- Brotherton M.S., van Breugel W., Stanford S.A., Smith R.J., Boyle B.J., Miller L., Shanks T., Croom S.M., Filippenko A.V. 1999, ApJ 520, L87
- Francis P.J., Hewett P.C., Foltz C.B., Chaffee F.H., Weymann R.J., Morris S.L. 1991, ApJ 373, 465
- Freeman K.C. 1970, ApJ 160, 811
- Hines D.C., Schmidt G.D., Smith P.S., Cutri R.M., Low F.J. 1995, ApJ 450, L1
- Hines D.C., Wills B.J. 1993, Rev.Mexicana Astron.Astrofis. 27, 149
- Hooper E.J., Impey C.D., Foltz C.B. 1997, ApJ 480, L95
- Kent S.M. 1985, ApJS 59, 115
- Kodama T., Arimoto N. 1997, A&A 320, 41
- Kodama T., Arimoto N., Barger A.J., Aragón-Salamanca A. 1998, A&A 334, 99
- Landolt A.U. 1992, AJ 104, 340
- Lilly S.J., Schade D., Ellis R., Le Fevre O., Brinchmann J., Tresse L., Abraham R., Hammer F. et al. 1998, ApJ 500, 75
- Lilly S.J., Tresse L., Hammer F., Crampton D., Le Févre O. 1995, ApJ 455, 108
- McLure R.J., Kukula M.J., Dunlop J.S., Baum S.A., O'Dea C.P., Hughes D.H. 1999, MNRAS 308, 377

Table 1. Summary of photometry of AX J131831+3341.

	<i>B</i> (mag)	<i>V</i> (mag)	<i>R</i> (mag)	<i>I</i> (mag)	<i>B</i> − <i>V</i> (mag)	<i>V</i> − <i>R</i> (mag)	<i>R</i> − <i>I</i> (mag)
Total (from UH88'')	21.23	21.08	20.00	18.96	0.15	1.08	1.04
Total (from Subaru)	...	21.06	20.04	1.02	...
Nucleus	...	22.61	22.26	21.77	...	0.35	0.49
Total − Nucleus	...	21.36	20.19	19.04	...	1.17	1.15
Region A	...	22.91	21.90	21.10	...	1.01	0.80
Region B	...	23.24	22.14	20.92	...	1.10	1.22

Predehl P., Schmitt J.H.M.M. 1995, A&A 293, 889

Risaliti G., Maiolino R., Salvati M. 1999, ApJ 522, 157

Sanders D.B., Soifer B.T., Elias J.H., Madore B.F., Matthews K., Neugebauer G., Scoville N.Z. 1988, ApJ 325, 74

Scheffler H., Elsässer H. 1988, Physics of the Galaxy and Interstellar Matter (Springer Verlag, Berlin)

Stocke J.T., Morris S.L., Gioia I.M., Maccacaro T., Schild R., Wolter A., Fleming T.A., Henry J.P. 1991, ApJS 76, 813

Ward M., Penston M.V., Blades J.C., Turtle A.J. 1980, MNRAS 193, 563

Willott C.J., Rawlings S., Blundell K.M., Lacy M. 2000, MNRAS in press

Winkler H. 1992, MNRAS 257, 677

Zheng Z., Wu H., Mao S., Xia X.-Y., Deng Z.-G., Zou Z.-L. 1999, A&A 349, 735

Figure Captions

Fig. 1. Deep R -band 4×4 binned image of AX J131831+3341 with a total exposure time of 1800 s. The field of view of the image is $24'' \times 24''$. North is up and east is to the left. We show the sky-subtracted image of the object with a surface brightness ranging from -3 times the standard deviation to $+9$ times the standard deviation as a gray scale with a linear scale. Regions A and B, where the colors of the extended component are measured, are indicated by rectangles.

Fig. 2. (a) R -band model image of AX J131831+3341 constructed from an ellipse fitting (see text for details). (b) Residual image after subtracting the model image from the original image. The field of view of the images and the gray scale levels are the same as in figure 1.

Fig. 3. V , R , and I band profiles of AX J131831+3341 along the major axis of the extended component. The profiles in the southeastern and northwestern directions are shown by the thick and thin solid lines, respectively. The thick and thin dashed lines for the R and V bands represent the sum of the fitted exponential-law profile and the PSF profile for the southeastern direction and for the northwestern direction, respectively.

Fig. 4. $V - R$ and $R - I$ colors of the nuclear (filled square) and the extended (region A: filled triangle, region B: filled pentagon, total—nucleus: filled circle) components of AX J131831+3341. The tracks of the elliptical and disk models with ages from 0.01 Gyr to 12 Gyr are indicated by the thick solid and dotted lines, respectively. The positions at an age of 6 Gyr are indicated by the tick marks on each track. The open circle represents the color of an average QSO SED (Francis et al. 1991). The pentagons show the colors of a power-law model with indices ($f_\nu = \nu^\alpha$) of $\alpha = -1.0, 0.0, 1.0$ from top to bottom. The dashed line indicates the expected colors for the average QSO SED with the absorption derived from the X-ray spectrum ($A_V = 1.1 - 5.9$ mag). The thick region of the dashed line shows an absorption larger than $A_V = 3.3$ mag, which was obtained for the nuclear component by assuming the typical optical to X-ray flux ratio of X-ray selected AGNs. The arrow represents the effect of reddening with A_V of 1 mag.

Fig. 5. R -band profiles of AX J131831+3341 in the southeastern and the northwestern directions (thick solid line) compared with those of QSO host galaxies at $z < 0.3$ (McLure et al. 1999) (thin solid lines). The best-fit model profiles of the QSO host galaxies at $z < 0.3$ are convolved with our PSF, and are corrected for K -correction and

surface brightness dimming to compare the profiles at $z = 0.653$.

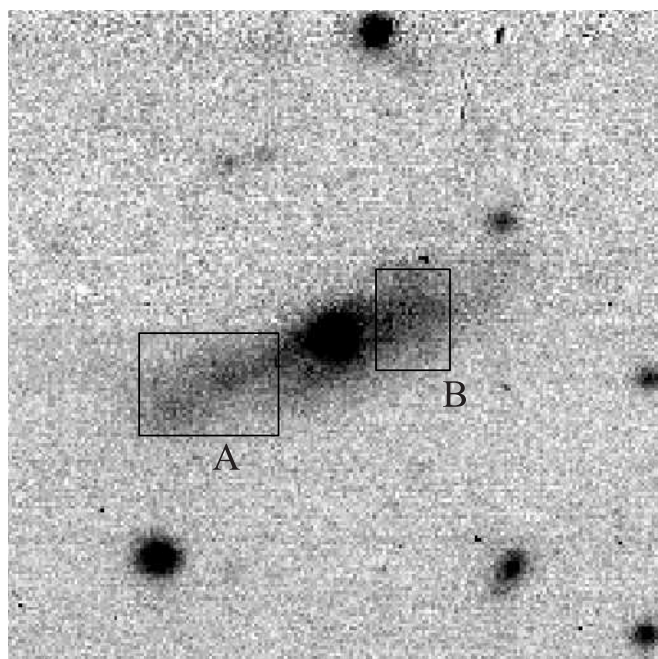


Fig. 1..

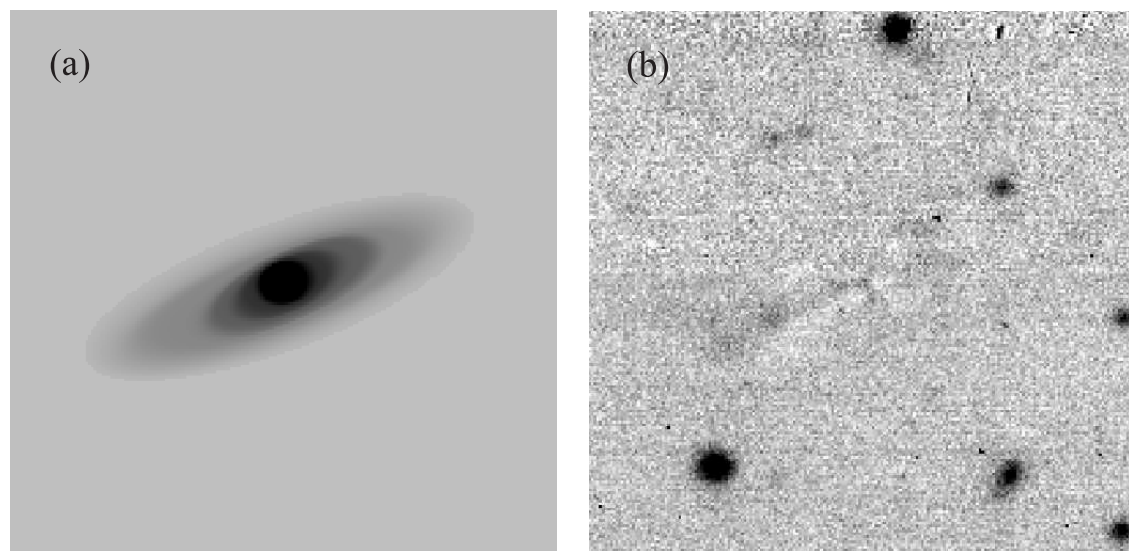


Fig. 2..

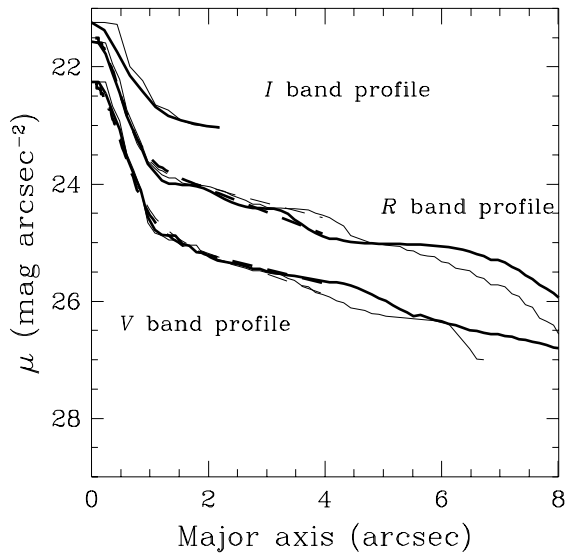


Fig. 3..

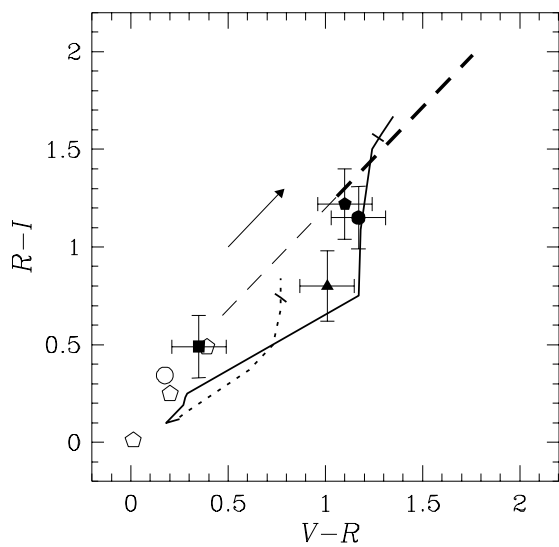


Fig. 4..

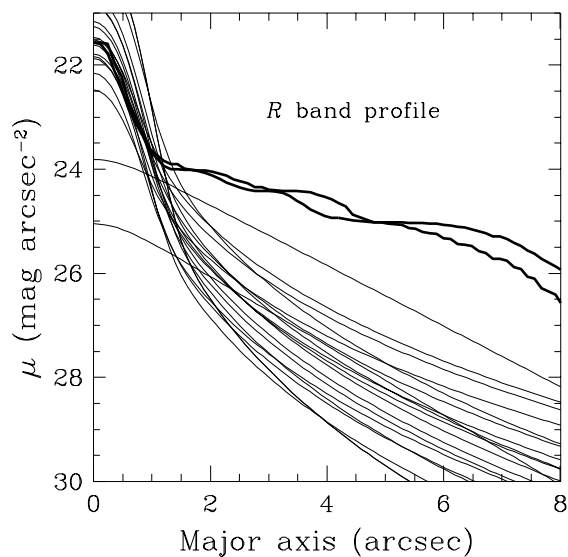


Fig. 5..